Magnetic and structural anisotropies of Co_2FeAl Heusler alloy epitaxial thin films

M.S. Gabor, T. Petrisor Jr., and C. Tiusan*
Technical University of Cluj-Napoca, Materials Science Laboratory, Cluj-Napoca, Romania. and Institut Jean Lamour, P2M, CNRS - Nancy University, Nancy, France.

M. Hehn
Institut Jean Lamour, P2M, CNRS - Nancy University, Nancy, France.

T. Petrisor
Technical University of Cluj-Napoca, Materials Science Laboratory, Cluj-Napoca, Romania.
(Dated: May 18, 2022)

This paper shows the correlation between chemical order, lattice strains and magnetic properties of Heusler Co_2FeAl films epitaxially grown on MgO(001). A detailed magnetic characterization has been performed using vector field magnetometery combined with numerical Stoner-Wohlfarth analysis. We demonstrate the presence of three types of in-plane anisotropies: one biaxial, as expected for the cubic symmetry, and other two uniaxial ones. The three anisotropies show different behavior with the annealing temperature. The biaxial anisotropy shows a monotonous increase. The uniaxial anisotropy, parallel with the hard biaxial axes, related to the chemical homogeneity, decreases, while the other, supposed to have magnetostatic origin, remains constant.

I. INTRODUCTION

Half metallic ferromagnets (HMFs) represent alternative candidates for magnetic electrodes in magnetic tunnel junctions (MTJs) and current-perpendicular-to-plane (CPP) spin valves (SVs). Having an energy gap around the Fermi level (E_F) in the minority spin band, theoretically, they are expected to provide 100% spin polarization. Among the HMFs, a special class is represented by the full Heusler alloys. These compounds are described by the formula X_2YZ, where X and Y are transition metals and Z is a main group *sp* element. Recent theoretical predictions[1, 2] indicate that the Co based full-Heusler alloys should behave like half metals even at room temperature. Presently, one of the most studied full Heusler alloys is the Co_2FeAl (CFA). It was demonstrated to provide giant tunneling magnetoresistance effects in magnetic tunnel junctions[3, 4] (MTJs) and has a low Gilbert damping [5]. While the low damping is essential for spin switching with low currents and spin torque oscillators it enhances the spin-torque induced mag-noise in CPP-GMR sensors. This is one of several reasons why CPP-GMR sensors are not yet competitive.

However, the integration of CFA as a ferromagnetic electrode in spintronic devices requires a precise knowledge and control of its magnetic properties. In this sense, one of the key parameters is the magnetic anisotropy. It should be large for magnetic storage and low for magnetic switching applications. Fundamentally, the magnetic anisotropy is directly related to the spin-orbit coupling relativistic effect. Therefore, modifications of the electronic structure in bulk, surface or interfaces are expected to lead to important changes in the magnetic anisotropy [6, 7].

The crystalline structure of Heusler alloys is cubic belonging to the $Fm\bar{3}m$ space group. Therefore, the (001) epitaxial films are expected to show an in-plane fourfold magnetic anisotropy. However, in case of Heusler alloys grown on GaAs (001) substrates [8–14] a dominant in plane uniaxial magnetic anisotropy (UMA) has often been reported. This uniaxial term can be reduced by buffering the GaAs substrate with MgO for Co_2MnSi (CMS) films [13] whereas in case of $Co_2Cr_{0.4}Fe_{0.4}Al$ (CCFA) films [10] the MgO buffering has no major effect. Uniaxial anisotropy contributions have been also reported on Heusler films deposited on sapphire substrates [15, 16], Si (111) [17], Ge(111)[18] or MgO (001) [19–21]. Moreover, extra UMAs have been reported not only on Heusler alloys but on different magnetic cubic crystal symmetry systems grown on various substrates [7]. The complex origin of this additional UMA is still under debate. Several mechanism are evoked as possible causes: symmetry breaking at atomic stepped substrates [22–24], anisotropic strain relaxation [25, 26], film morphology [27, 28] or self-shadowing effects in oblique deposition [29].

In this paper we report a detailed study on the structural/crystallographic and magnetic properties of CFA thin films epitaxially grown on MgO buffered MgO(001) single crystalline substrates. Our analysis demonstrates that a direct correlation exists between the in-plane magnetic anisotropy and the structural evolution of the CFA film, tuned by annealing. Moreover, we illustrate here that magnetic analysis, dedicated to extract the different anisotropy terms of epitaxial CFA films, can be successfully performed within a Stoner-Wohlfarth (S-W) coherent rotation model which includes a biaxial and two uniaxial anisotropy contributions.

* Electronic mail: coriolan.tiusan@phys.utcluj.ro

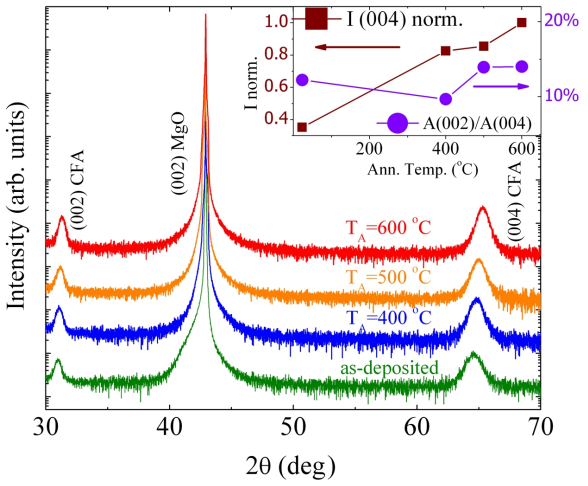

FIG. 1. $2\theta - \omega$ diffraction pattern for the MgO buffered CFA films as a function of annealing temperature. The inset shows the evolution of the CFA 004 peak normalized intensity (I(004))and the ratio of the integral intensities of the (002) and (004) CFA peaks (A(002)/A(004)), with respect to the annealing temperature.

II. EXPERIMENTAL

The CFA films were grown on MgO buffered MgO (001) single crystal substrates using RF magnetron sputtering. The base pressure in the deposition chamber was better than of 3×10^{-8} Torr. Prior to deposition the substrates were *in-situ* degassed at 600°C. Then, a 10 nm thick MgO buffer layer has been deposited at room temperature (RT) by RF sputtering from a MgO polycrystalline target under an Ar pressure of 5.0 mTorr. The MgO layer improves the flatness quality of the substrate and traps the residual carbon preventing further diffusion across the stack during subsequent annealing stages. After the buffer layer deposition, a 55 nm thick CFA film has been sputtered at room temperature in RF plasma from a stoichiometric target ($Co_{50\%}Fe_{25\%}Al_{25\%}$) under 1.0 mTorr of Ar. Finally, the films were caped with 5 nm of MgO. After the growth of the stack, the films were flash annealed for 10 minutes in a vacuum better than 3×10^{-8} Torr at 400, 500 and 600°C.

The structural properties of the samples have been analyzed by X-Ray Diffraction (XRD) using a high-resolution four circle diffractometer. The magnetic characteristics were investigated by vibrating sample magnetometry (VSM) equipped with vector field characterization option.

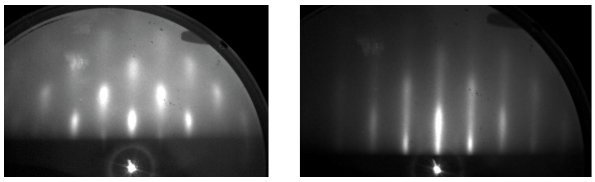

FIG. 2. RHEED patterns recorded in for samples as-deposited (left hand side) and annealed at 600 °C (right hand side), showing the improvement of crystallographic quality with annealing.

III. RESULTS AND DISCUSSIONS

A. Structural properties

Figure 1 shows X-ray $2\theta - \omega$ (out-of-plane) diffraction patterns for MgO buffered CFA films: as-deposited and annealed at 400, 500 and 600 °C. The analysis of the XRD patterns illustrates that in addition to the peak corresponding to the MgO substrate all the samples exhibit only the (002) and (004) peaks of the CFA. Theoretically, from the chemical order point of view, the CFA crystal may be in a perfectly chemically ordered $L2_1$ phase, a $B2$ phase characterized by total disorder between Fe an Al while Co atoms occupy regular sites, and the $A2$ phase which is totally disordered with respect to Fe, Al and Co. In our samples, the presence of the (002) CFA reflection indicates that the films contain the $B2$ phase. The perfectly ordered $L2_1$ structure would be characterized by the presence of superlattice reflections like (111) or (311) [30]. In order to test the occurrence of superlattice peaks we performed in-plane ϕ scan measurements. Within the accuracy of the measurements, no $L2_1$ type reflections could be observed. This suggests that in our samples the $B2$ structural phase is dominating. Polar figures (not shown here) confirm the epitaxial growth of the CFA films according to the expected CFA(001)[110]||MgO(001)[100] epitaxial relation.

The inset in the figure 1 shows the evolution of the normalized intensity I(004) of the (004) CFA reflection versus the annealing temperature. The normalized intensity shows a monotonic increase with the annealing temperature, with a significant jump for the sample annealed at 400 °C relative to the as deposited one. This implies an important improvement of the structure at atomic level for the annealed samples. It is reasonable to assume that the as-deposited samples contain regions with structural/crystalline disorder which vanishes upon annealing. This represents a transition from short range to long range crystallographic order. RHEED analysis, performed on similar samples transferred and annealed in an UHV chamber, supports this fact and also indicates an overall improvement of the crystallization degree (see figure 2).

The (002) reflection is characteristic to the $B2$ structure. Thus, the integrated peak intensity ratio

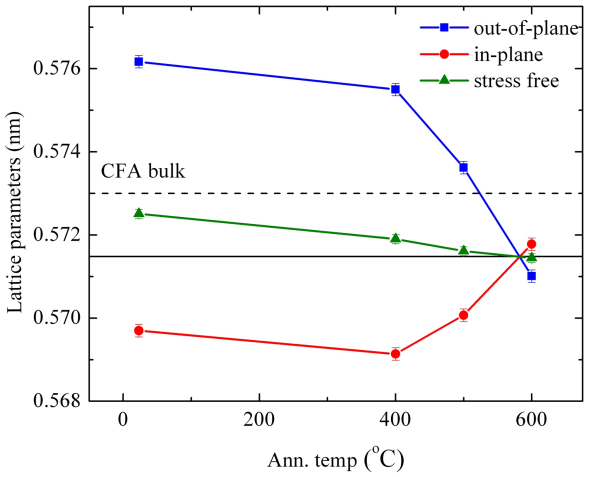

FIG. 3. Evolution of the out-of-plane and in-plane lattice parameters for the versus the annealing temperature. The stress-free lattice parameter is also plotted. The dashed lines represents the bulk $L2_1$ ordered CFA lattice parameter. The horizontal continuous line marks the position of the stress free lattice parameter (a_0^{600}) after annealing at 600 °C.

A(002)/A(004) represents a measure of the degree of order on Co sites. This ratio, shown in the inset of figure 1, exhibits a decrease for the 400 °C annealed sample, relative to the as deposited one, although the I(004) intensity increases significantly. This may be related to the presence of regions with structural disorder in the as-deposited sample that, with annealing, crystallize in the chemically disordered $A2$ structure, therefore increasing I(004) and reducing the A(002)/A(004) ratio. As the annealing temperature is further increased, the $A2$ phase gradually evolves towards the better chemically ordered $B2$ one leading to an increase of the A(002)/A(004) ratio.

The in-plane ($a_\parallel$) and out-of-plane ($a_\perp$) lattice parameters of the epitaxial CFA films were determined by performing reciprocal lattice scans. First, we carried out an l-scan (2θ-θ symmetrical geometry) around the (002) node of the CFA reciprocal lattice and obtained the d_{002} distance, which allows us to calculate $a_\perp$. Using this l coordinate we performed an h=k scan ($\omega-2\theta$ asymmetrical geometry) around the (224) CFA reciprocal lattice node and obtained the d_{224} distance, that we used to derive $a_\parallel$. The obtained values are depicted in figure 3.

From figure 3 one can observe that the as-deposited film experiences a relative strong tetragonal distortion. As the annealing temperature is increased the distortion is relaxed by formation of misfit dislocations. Periodic arrays of columnar misfit dislocations across all the thickness of the CFA film have been observed on films annealed at 600 °C, from phase analysis of cross-section Transmission Electron Microscopy (TEM) images (not presented here). The XRD investigations demonstrates that the lattice parameter after annealing is smaller than the bulk value of the perfectly $L2_1$ ordered cell. This could be explained by the presence of some $A2$ type disorder, as already reported in literature [31].

Our analysis illustrates a totally counter intuitive evolution of the lattice parameters with annealing. Due to the in-plane tensile stress between the film and the MgO buffer, one would expect that the in-plane lattice parameter to be larger than the out-of-plane one and, eventually, the distortion to be relaxed with annealing by plastic relaxation (e.g. formation of misfit dislocations). Most likely, the unusual lattice distortion is connected to the growth method. As illustrated in the literature [32], during the growth of the films by sputtering, the bombardment of the film by energetic neutral atoms reflected of the target can create point defects in the lattice or regions with structural disorder. These will generate local strain fields which can disturb the crystallization and may give rise to lattice distortion as the one observed in our films.

To gain further insight of the strain evolution with the annealing temperature we have plotted in figure 3 the stress free lattice parameter of CFA, calculated according to the elasticity theory:

$$a_0 = \frac{C_{11}a_\perp + 2C_{12}a_\parallel}{C_{11} + C_{12}}, \qquad (1)$$

where C_{11} and C_{12} are the elastic stiffness constants.

The stiffness constants were calculated using the elastic package implemented in the *ab-initio* FPLAPW Wien2k code [33]. In order to calculate the three independent elastic constants C_{11}, C_{12} and C_{44} three types of strains corresponding to highly symmetric types of deformation have been considered: isotropic deformation by varying the cubic volume, tetragonal volume-conservative distortion and rhombohedral distortion. The total energy of the system is calculated $ab-initio$ for each distorted configuration and then fitted with polynomial models. From this analysis one gets a set of equations allowing the determination of the full elastic tensor components. Using this formalism, we obtain the following values for the elastic constants: C_{11}=253 GPa, C_{12}= 165 GPa, C_{44}=153 GPa.

The theoretical temperature variation of the lattice parameter is calculated using the $ab-initio$ extracted values for the elastic constants and the experimental temperature variation for $a_\perp$ and $a_\parallel$. If one assumes only elastic nature stress in the films then, if the in-plane lattice parameter changes, the out-of-plane parameter should change accordingly so that the stress free lattice parameter to remain constant. As can be seen in the figure 3 the stress-free lattice parameter of the as-deposited film is increased by 0.2%, with respect to the one corresponding to the 600 °C annealed film.The expansion is progressively reduced with annealing once the crystallization and chemical order is enhanced. This verifies that for as-deposited and low temperature annealed samples, there is stress related to crystallographic point defects, poorly crystalized regions or even to regions of different chemical order.

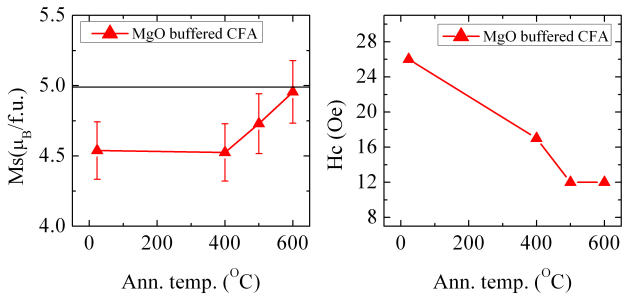

FIG. 4. Evolution of the saturation magnetization and coercive field, measured along the easy axis, as a function of annealing temperature for MgO buffered CFA films.

B. Magnetic properties

In order to study the magnetic properties of our films, we performed hysteresis loops and angular remanence magnetization measurements (ARM) at room temperature with the magnetic field applied parallel to the film surface.

Figure 4 shows the saturation magnetization (Ms) and coercive field (Hc), measured along the [-110] crystallographic direction, as a function of annealing temperature. The saturation magnetization for the as-deposited and 400 °C annealed films has roughly the same value which, for higher annealing temperatures, evolves towards the theoretically predicted one [1]. This confirms that the structural evolution of the annealed samples between as-deposited to 400°C is not related to a significant stoichiometry variation (accompanied by a change in Ms). This is most likely a crystallization related effect. As supported by structural analysis (previous paragraph), practically, the system evolves from a local (short range) crystallographic order towards a long range crystalline order. However, this transition from disordered towards crystallographically ordered and chemically disordered $A2$ phase does not affect the magnetization. In average, within the regime of the chemical disorder, the total magnetic moment remains constant. An accurate quantitative temperature variation of the Ms is difficult due to the large error bars (see figure 4). However, beyond 400°C, the increase in Ms can be attributed to the improvement of the chemical order and local stoichiometry. This leads to a change in the saturation magnetization, as reflected by the curve plotted in figure 4.

The decrease of Hc with the annealing is consistent with the reduction of the defect density with enhancing the crystalline quality.

Magnetic hysteresis loops, recorded along the main crystallographic directions, are shown in figure 5 for the film deposited on MgO buffer layer and annealed at 400 °C.

All samples show easy magnetization axes along CFA [110] and [-110] crystallographic directions and hard axes parallel to [100] and [010]. From figure 5 one can observe

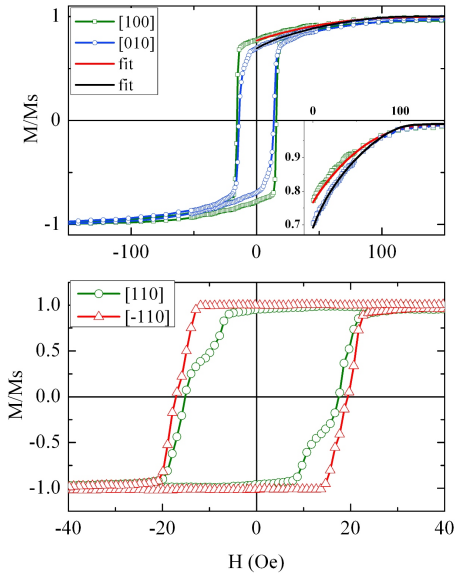

FIG. 5. Magnetization loops along the main crystallographic axes for the film annealed at 400 °C. The inset shows a zoom of the data used for numerical fitting and the result of the fit (continuous lines).

that the two easy axes are not equivalent. Inequivalent hard axes are also observed. This leads us to conclude that, in the case of CFA films deposited on MgO, the biaxial anisotropy is altered by the superposition of two uniaxial in-plane anisotropies: one with the easy axis parallel to [110] direction and the other parallel with the easy axis parallel to the [100] direction.

To get quantitative insight into the magnetic properties of the CFA films, we performed numerical simulations based on the macrospin Stoner-Wohlfarth (S-W) formalism [34]. We defined a total energy functional containing anisotropy energy terms related to one in-plane biaxial anisotropy and two in-plane uniaxial anisotropies rotated by 45 degrees one from each other. This writes as:

$$E = \frac{K_4}{4}\sin^2(2\theta) + K_U^1 \sin^2\left(\theta + \frac{\pi}{4}\right) + K_U^2 \sin^2\left(\theta + \frac{\pi}{2}\right) - \mu_0 M s H \cos(\phi - \theta), \quad (2)$$

where Ms is the saturation magnetization, H is the applied field, θ and ϕ are the angles of the magnetization and applied field relative to the easy axis direction (i.e. [110]), K_4 is the biaxial anisotropy constant, K_U^1 is the uniaxial anisotropy constant parallel to the biaxial hard axis and K_U^2 is the uniaxial anisotropy constant parallel with the biaxial easy axis.

In order to determine the anisotropy constants for these samples, we took up to four hysteresis loops, measured in the proximity of the hard axes, and fitted them simultaneously within the S-W coherent rotation model, using as parameters the anisotropy constants. When fitting the hysteresis curves, we limited ourselves to the

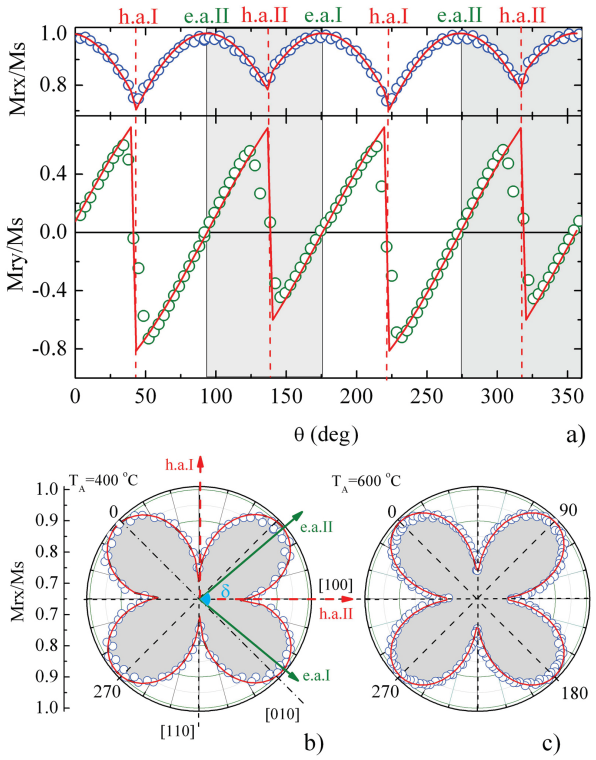

FIG. 6. Angular remanence magnetization measurements for the sample annealed at 400 °C a) and b), and for the sample annealed at 600 °C c). The symbols represents experimental data while lines are numerical simulations according to the model described in text. The position of the overall easy and hard axes is also represented (a).

reversible part of the M-H loop for which we can assume coherent rotation: i.e. from saturation towards zero applied field (see inset of figure 5).

With the values obtained for the anisotropy constants (parameters) we simulated the 'theoretical' ARM curves. The results are illustrated in figure 6. One can observe a very good agreement between the experimental points and the simulations (solid lines).

In the case of the 400 °C annealed sample the effect of UMA parallel with the biaxial hard axis is to rotate the onward the overall easy axes, to an angle δ different of 90° (figure 6 (b)). The effect of the UMA parallel with the biaxial easy axis is to increase the area of the lobes in the ARM polar plot. This can be easily verified in simulations by setting $K_U^2 = 0$. From figure 6 (c) one can see that for high enough annealing temperatures the effect of UMA parallel with the hard axis vanishes.

The values of the anisotropy fields deduced from the numerical fitting are shown in figure 7. The four-fold anisotropy field (K_4/Ms) increases with annealing, the K_U^1/Ms decreases to negligible values for annealing temperatures above 400 °C, while K_U^2/Ms remains independent of annealing temperature. Is to be noted that in the case of the as-deposited sample , we were not able to fit the experimental magnetization curves within the framework of our simple model. This is most likely due to the complex crystallographic structure (higher degree of crystallographic disorder) observed for this sample, as we mentioned in the first section.

One of the most interesting features reported in figure 7 is the fact that the small amplitude K_U^2/Ms remains practically independent of the annealing temperature. We suppose that this temperature-independent uniaxial anisotropy has a magnetostatic origin related to stepped substrates due to a small miscut [35] along the [100] substrate crystallographic direction corresponding to the [110] CFA one. To verify this assumption, we built samples using a 20 nm thick Cr buffer layer. In these samples the substrate morphology influence is expected to vanish. Indeed, for these Cr buffered samples we did not observed any UMA parallel with the biaxial anisotropy easy axes: the two fourfold easy axes being equivalent. A figure of merit of our analysis model is the capability to extract with accuracy small anisotropy constants and to show their invariance with the temperature.

In order to elucidate the origin of the UMA parallel with the biaxial hard axes we extensively performed XRD analysis. However, within the accuracy of the XRD measurements we could not confirm any correlation between the UMA and possible in-plane structural anisotropy or anisotropic strain relaxation. By increasing the annealing temperature from 400 °C to 500 °C the UMA practically vanishes. The only difference between the sample annealed at 400 °C and the one annealed at 500 °C is the degree of chemical ordering (see figure 1). Therefore, we argue that this UMA is the result of an anisotropic chemical disorder in the films. The presence of chemical disordered domains, separated irregularly along the MgO [110] and MgO [1-10] crystallographic axes and vanishing for high annealing temperatures (> 550 °C) was already identified [36] using low energy electron diffraction (LEED) in the case of the related $Co_2Cr_{0.6}Fe_{0.4}Al$ Heusler compound grown on MgO (001). This result is in agreement and comes to further sustain our conclusion that the uniaxial magnetic anisotropy is a result of an anisotropic chemical disorder in the films. In this point we have no clear explanation why the favored direction of this UMA easy axis is [100] against [010]. Further explanation would require identifying of some symmetry breaking mechanism as, for example, the miscut of the substrate.

In figure 7 we illustrate the evolution of the anisotropy field with the annealing temperature. One can see that the K_4/Ms increases continuously with annealing. A first origin of this increase could be correlated to the improvement of the chemical order/stoechiometry within the cubic symmetry of the CFA films with annealing, as confirmed by the decrease of the uniaxial K_1^U/Ms. However, at annealing temperatures above 500°C the K_1^U/Ms is practically zero, whereas the K_4/Ms continues to increase. Therefore, an additional mechanism

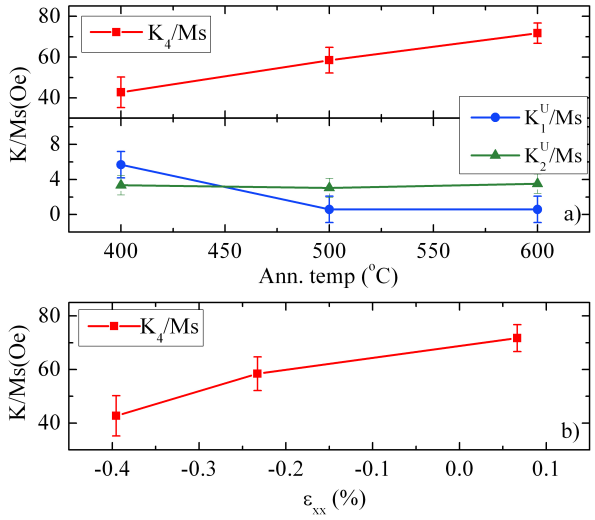

FIG. 7. Evolution of the cubic (K_4/Ms) and uniaxial (K_U^1/Ms and K_U^2/Ms) anisotropy fields with annealing temperature for the samples deposited on MgO buffered substrates (upper part). The variation of the four-fold anisotropy field with the in-plane biaxial strain (lower part).

for the temperature dependence of the biaxial anisotropy has to be considered. It is related to the evolution in temperature of the in-plane biaxial strain ($\varepsilon_{xx} = (a_{\parallel} - a_0^{600})/a_0^{600}$). The biaxial anisotropy constant is connected to the in-plane biaxial strain through the magneto-elastic coupling parameters [37]. To our knowledge, there are no reports in the literature estimating the values of these constants. This would have allowed us to quantify and extract precisely the strain contribution to the total variation of K_4/Ms with the annealing temperature. However, in the figure 7(b) we plot the biaxial anisotropy constant, extracted from magnetic analysis, as a function of the in plane biaxial strain, extracted from X ray measurements. This confirms a direct correlation between four-fold anisotropy and biaxial strain, without being able to discriminate between the relative ratio of the strain and the chemical order contributions.

Our analysis provides anisotropy constants values, especially for the biaxial anisotropy, which are in good agreement with the ones reported in literature for related Co_2MZ Heusler compounds (for a list of available data see the review paper [38]). Moreover, a recent paper by Trudel et. al. [21] illustrate by a complex study the presence and evolution with the annealing of a biaxial and uniaxial anisotropy in $Co_2Fe_{0.5}Al_{0.5}Si$ grown on MgO (001). Our data are in good qualitative agreement with the ones reported by the authors, quantitative differences being only related to electronic structure direct effects in our Co_2FeAl samples without Si substitutions and to the difference in the ordering degree of our Co_2FeAl (only B2) with respect to their $Co_2Fe_{0.5}Al_{0.5}Si$ (B2 evolution towards $L2_1$).

IV. CONCLUSION

In this paper we presented a detailed structural and magnetic analysis of CFA thin films epitaxially grown on MgO(001) substrates. The evolution of the chemical order and the lattice parameters with the annealing temperature has been studied. An exhaustive magnetic characterization of the CFA films has been performed using vector field VSM magnetometery combined with numerical Stoner-Wohlfarth analysis. This allowed to demonstrate the presence of three types of in-plane anisotropies: biaxial (as expected for the cubic symmetry) and two uniaxial contribution parallel with the biaxial easy and hard axes. The biaxial anisotropy shows a monotonous increase with the annealing. One of the uniaxial anisotropy, related to the chemical order, decreases while the other, supposed to have magnetostatic origin, remains constant with the annealing. These behaviors have been correlated to the chemical homogeneity and strain evolution within the films.

ACKNOWLEDGMENTS

This work has been partially supported by CNCSIS UEFISCSU, project number PNII IDEI No.4/2010, code ID-106 and by POS CCE ID. 574, code SMIS-CSNR 12467. C. Tiusan acknowledges to the SPINCHAT project ANR- 07-BLAN-341.

[1] I. Galanakis, P. H. Dederichs, and N. Papanikolaou, Phys. Rev. B **66**, 174429 (2002).
[2] S. Picozzi, A. Continenza, and A. J. Freeman, Phys. Rev. B **66**, 094421 (2002).
[3] W. Wang, H. Sukegawa, R. Shan, S. Mitani, and K. Inomata, Applied Physics Letters **95**, 182502 (2009).
[4] W. Wang, E. Liu, M. Kodzuka, H. Sukegawa, M. Wojcik, E. Jedryka, G. H. Wu, K. Inomata, S. Mitani, and K. Hono, Phys. Rev. B **81**, 140402 (2010).
[5] S. Mizukami, D. Watanabe, M. Oogane, Y. Ando, Y. Miura, M. Shirai, and T. Miyazaki, Journal of Applied Physics **105**, 07D306 (2009).
[6] D. Sander, Rep. Prog. Phys. **62**, 809 (1999).
[7] C. A. F. Vaz, J. A. C. Bland, and G. Lauhoff, Rep. Prog. Phys. **71**, 056501 (2008).
[8] T. Ambrose, J. J. Krebs, and G. A. Prinz, Applied Physics Letters **76**, 3280 (2000).
[9] F. Y. Yang, C. H. Shang, C. L. Chien, T. Ambrose, J. J. Krebs, G. A. Prinz, V. I. Nikitenko, V. S. Gornakov, A. J. Shapiro, and R. D. Shull, Phys. Rev. B **65**, 174410 (2002).

[10] T. Yano, T. Uemura, K. i. Matsuda, and M. Yamamoto, Journal of Applied Physics **101**, 063904 (2007).

[11] A. Hirohata, H. Kurebayashi, S. Okamura, M. Kikuchi, T. Masaki, T. Nozaki, N. Tezuka, and K. Inomata, Journal of Applied Physics **97**, 103714 (2005).

[12] M. Hashimoto, J. Herfort, H.-P. Schönherr, and K. H. Ploog, Journal of Applied Physics **98**, 104902 (2005).

[13] S. Kawagishi, T. Uemura, Y. Imai, K.-I. Matsuda, and M. Yamamoto, Journal of Applied Physics **103**, 07A703 (2008).

[14] W. H. Wang, M. Przybylski, W. Kuch, L. I. Chelaru, J. Wang, Y. F. Lu, J. Barthel, H. L. Meyerheim, and J. Kirschner, Phys. Rev. B **71**, 144416 (2005).

[15] H. Schneider, C. Herbort, H. A. G Jakob1, S. Wurmehl, and C. Felser, J. Phys. D: Appl. Phys. **40**, 1548 (2007).

[16] M. Belmeguenai, F. Zighem, T. Chauveau, D. Faurie, Y. Roussigné, S. M. Chérif, P. Moch, K. Westerholt, and P. Monod, Journal of Applied Physics **108**, 063926 (2010).

[17] S. Yamada, K. Hamaya, K. Yamamoto, T. Murakami, K. Mibu, and M. Miyao, Applied Physics Letters **96**, 082511 (2010).

[18] K. Kasahara, K. Yamamoto, S. Yamada, T. Murakami, K. Hamaya, K. Mibu, and M. Miyao, Journal of Applied Physics **107**, 09B105 (2010).

[19] W. Wang, H. Sukegawa, R. Shan, T. Furubayashi, and K. Inomata, Applied Physics Letters **92**, 221912 (2008).

[20] S. Trudel, J. Hamrle, B. Hillebrands, T. Taira, and M. Yamamoto, Journal of Applied Physics **107**, 043912 (2010).

[21] S. Trudel, G. Wolf, J. Hamrle, B. Hillebrands, P. Klaer, M. Kallmayer, H.-J. Elmers, H. Sukegawa, W. Wang, and K. Inomata, Phys. Rev. B **83**, 104412 (2011).

[22] R. K. Kawakami, E. J. Escorcia-Aparicio, and Z. Q. Qiu, Phys. Rev. Lett. **77**, 2570 (1996).

[23] M. Mathews, F. M. Postma, J. C. Lodder, R. Jansen, G. Rijnders, and D. H. A. Blank, Applied Physics Letters **87**, 242507 (2005).

[24] J. Chen and J. L. Erskine, Phys. Rev. Lett. **68**, 1212 (1992).

[25] Y. B. Xu, D. J. Freeland, M. Tselepi, and J. A. C. Bland, Phys. Rev. B **62**, 1167 (2000).

[26] O. Thomas, Q. Shen, P. Schieffer, N. Tournerie, and B. Lépine, Phys. Rev. Lett. **90**, 017205 (2003).

[27] R. Moroni, D. Sekiba, F. Buatier de Mongeot, G. Gonella, C. Boragno, L. Mattera, and U. Valbusa, Phys. Rev. Lett. **91**, 167207 (2003).

[28] Q. feng Zhan, S. Vandezande, C. V. Haesendonck, and K. Temst, Applied Physics Letters **91**, 122510 (2007).

[29] L. Abelmann and C. Lodder, Thin Solid Films **305**, 1 (1997).

[30] K. Ziebeck and N. S. P.J. Webster: Landolt-Börnstein, (1986).

[31] K. Inomata, S. Okamura, A. Miyazaki, M. Kikuchi, N. Tezuka, M. Wojcik, and E. Jedryka, J. Phys. D: Appl. Phys. 39 816 **39**, 816 (2006).

[32] Y. Huttel, J. I. Cerdá, J. L. Martínez, and A. Cebollada, Phys. Rev. B **76**, 195451 (2007).

[33] P. Blaha, K. Schwarz, G. K. H. Madsen, D. Kvasnicka, and J. Luitz, *Wien2k, An Augmented Plane Wave Local Orbitals Program for Calculating Crystal Properties*, edited by K. Schwartz (Technical University of Wien, Austria, 2001).

[34] E. C. Stoner and E. P. Wohlfarth, Phil. Trans. R. Soc. Lond. A **240**, 599 (1948).

[35] A. Encinas-Oropesa and F. N. V. Dau, Journal of Magnetism and Magnetic Materials **256**, 301 (2003).

[36] J.-P. Wstenberg, J. Fischer, C. Herbort, M. Jourdan, M. Aeschlimann, and M. Cinchetti, Journal of Physics D: Applied Physics **42**, 084016 (2009).

[37] P. Bertoncini, P. Wetzel, D. Berling, A. Mehdaoui, B. Loegel, G. Gewinner, R. Poinsot, and V. Pierron-Bohnes, Journal of Magnetism and Magnetic Materials **237**, 191 (2001).

[38] S. Trudel, O. Gaier, J. Hamrle, and B. Hillebrands, Journal of Physics D: Applied Physics **43**, 193001 (2010).